On a Few Superficial Presentations of Ultra-Weak Photon Emission of Human: an Analytical Hypothesis

Daqing Piao [1,2] PhD

[1] School of Electrical and Computer Engineering, Oklahoma State University, Stillwater, OK 74078, USA

[2] Department of Veterinary Clinical Sciences, Center for Veterinary Health Sciences, Oklahoma State University, Stillwater, OK 74078, USA

Abstract:

Ultra-weak photon emissions (UPEs) including those from human have been experimented for decades. The photo-genic origin of UPE has also been attributed to the oxidative stress or free radical production that is unique to metabolically active states of biological organisms. However, there are considerable gaps in quantitative understanding of UPE. In this work, I propose an analytical framework of hypothesis for the initial objective of modeling a few superficial presentations of UPE of human, including the systematic dependency on age, the diurnal variation, and the geometric asymmetry associated with serious asymmetrical pathological conditions. The hypothesis which is currently limited to human assumes a new form of energy state, termed vivo-nergy, which resides only in metabolically active organisms that are also under neuronal control. The hypothesis projects a decrease of the vivo-nergy in human during growth beyond puberty, with the rate of decrease dictated by a critical time-scale---the age of the first opposite-sex sexual intercourse (FOSSI). The hypothesis also proposes a modification of the vivo-nergy by the phases

 doi:10.20944/preprints201810.0458.v1

of systematic or homeostatic physiology. The hypothesis further postulates that the deviation of the physiology-modified vivo-nergy from the pre-puberty level is deteriorated by acquired organ-specific pathological conditions. Any reduction of vivo-nergy from the pre-puberty level is hypothesized to proportionally cause oxidative stress that functions as the physical source of UPE. The resulted steady-state diffusion of the photon emitted from a photo-genic source of UPE in a human geometry simplified as a homogeneous spherical domain is modeled by photon diffusion principles incorporating an extrapolated zero-boundary condition. The age and systematic physiology combined determines the intensity of the centered physiological photo-genic source. The acquired (single) pathology sets both the intensity and the off-center position of the (single) pathological photo-genic source. When the age-related, physiology-commanded, and pathology-controlled modifications of the photo-genetic sources are implemented in the photon diffusion model, the photon fluence rate at the surface of the simplified human-representing spherical domain reveals the dependency on age, the temporal variation corresponding to systematic physiology, and the geometric asymmetry associated with significant asymmetric pathological condition as reported previously for UPE. The hypothesis, as it provides analytical conveniences for quantitative estimation of UPE patterns, may be useful to further model-based interpretation of the spatial-temporal characteristics of UPE.

Keywords: ultra-weak photon emission; age; temporal variation; asymmetry; analytical model; photon diffusion.

Preprints (www.preprints.org) | NOT PEER-REVIEWED | Posted: 19 October 2018 doi:10.20944/preprints201810.0458.v1

1. Introduction

Ultra-weak photon emission (UPE) [1] has been investigated over several decades under a variety of terms including the following that have appeared chronically: weak luminescence [2], low-level chemiluminescence [3], spontaneous chemiluminscence [4], biophoton(s) emission [5, 6], ultra-weak bioluminescence [7], autoluminescence [8], spontaneous ultra-weak light emission [9], etc. The spectrum of UPE interestingly covers the visible light and extends to ultraviolet and near-infrared bands [3, 5, 10-18]. The commonly reported UPE intensity is 100s of photons per second per square centimeter [6, 19-22]. For a photon at the visible wavelength of 500nm, a photon count rate of 100 photons per second per square centimeter corresponds to an irradiance of $3.98 \times 10^{-17} W \cdot cm^{-2}$ or $\sim 0.04 fW \cdot cm^{-2}$. This irradiance is comparable to the photon fluence rate measured at 10cm from a source of 1μW power in an unbounded homogeneous tissue medium having an absorption coefficient of 0.106cm^{-1} and a reduced scattering coefficient of 10cm^{-1}. The extremely small intensity makes UPE challenging to detect without completely darkened-out environment and highly sensitive photon detecting devices. The difficulty of detecting UPE also hinders the mechanism exploration beyond the known association of UPE with the oxidative stress [23] that is magnified by metabolic demands.

Although the photo-genic pathways of UPE are less specified, the characteristics of UPE regarding diffuse light emission are clearly inferred. A particularly robust observation of diffuse light emission properties of UPE was made from human hand by Nakamura and Hiramatsu [19]. In the presence of an air layer between the palm and the glass window of a photomultiplier tube (PMT), about 100 UPE photon counts per second was obtained, while in the absence of air layer by the contact of PMT with the palm through mineral oil, about 200 UPE photon counts per second was obtained. Similar level of UPE photon counts was obtained by water-immerged contact of

Preprints (www.preprints.org) | NOT PEER-REVIEWED | Posted: 19 October 2018 doi:10.20944/preprints201810.0458.v1

PMT with the palm or direct contact of the PMT glass window with the palm. The absence of air layer was justified as the sole attributer of the enhanced UPE intensity. That observation supported the notion that the UPE must have originated inside the skin. If the light of UPE originates inside the tissue, it will propagate within the tissue and evade the tissue when encountering a boundary. A better matching of the refractive index of the two media across the boundary will reduce the loss of the photons crossing the boundary and thus increase the UPE intensity measured on the surface. The enhancement of UPE by refractive index matching at the boundary is a boundary-value presentation common to light diffusion.

The variations of UPE intensity in association with normal physiological phases or environmental influences have been reported on different temporal scales. Diurnal rhythms of UPE of human have been linked to the systematic changes in energy metabolism inherent to a circadian cycle [24]. Frequency analysis of the UPE intensity revealed spectral components with longer-than-24-hours temporal characteristics ranging from 7-days to 270-days [6, 25]. Seasonal variation of UPE intensity [20, 25, 26] revealed as high as 4-folds of changes over year-long measurements with the lowest intensity in the autumn and the highest intensity appearing 6-months apart from the autumn. The UPE has also manifested gender and age-related variations [22, 27-30]. The UPE intensity was higher among males than among females, and higher in adults than in children. The aged male adult had ~40% higher UPE intensity than the aged female adult [27]. The UPE of both male and female started to increase by the age of 11-14 and stabilize at ages around 50 [27]. These findings indicate that measuring UPE can potentially provide insight into the homeostatic state or systematic stage, as well as the harmonic correlation between the human body and the environment that is regarded fundamental to some alternative medical practices [31]. Deviations of UPE

Preprints (www.preprints.org) | NOT PEER-REVIEWED | Posted: 19 October 2018 doi:10.20944/preprints201810.0458.v1

intensity from these healthy temporal rhythms thus may render information of the deviation of the systematic or homeostatic physiological states from the normal levels.

The temporal variations of the human UPE intensity of normal physiological states also infer that, a human state departing significantly from healthy conditions due to acquired pathology may reveal a variation of UPE intensity that is much stronger than that of a systematic cause. An acquired pathology that is site-specific could also cause the UPE pattern to be altered from a healthy balanced or symmetric configuration. A superficial presentation of UPE caused by acquired pathology will likely be the breaking of the systematic symmetry of UPE. A multiple sclerosis case was found to give ~200 counts/second in the right hand and ~300 counts/second in the left hand [6]. For hemiparesis patients, the hand of hemiparesis aspect emitted less UPE photons in comparison to the contra-lateral normal hand [32], and acupuncture treatment reduced dramatically the left-right asymmetry of UPE. The left-right asymmetry of UPE in a mouse model of human breast cancer [16] became more pronounced as the tumor load in the right axillary increased versus the contra-lateral normal control. These reports suggest that the left-right asymmetry of UPE correlates with the left-right difference on the pathological conditions.

The experimental observations of the physicality of UPE have substantiated the potential of UPE for applications including non-invasive assessment of the health [33]. However, there are considerable gaps in quantitative understanding of UPE, in terms of model-based accounting of the UPE patterns. Model-based thus quantitatively-rendered interpretation of the UPE patterns could foster experimental explorations that can target specific mechanism discovery of UPE. In this work, I propose an analytical framework of hypothesis for the initial objective of, for the first time, modeling a few superficial presentations of UPE of human including the systematic dependency on age, the diurnal variation, and the geometric asymmetry associated with serious

 doi:10.20944/preprints201810.0458.v1

asymmetrical pathological conditions. The hypothesis assumes a new form of energy state, termed "vivo-nergy," which resides only in metabolically active organisms that are also under neuronal control. The hypothesis projects a decrease of the vivo-nergy in human during growth beyond puberty, with the rate of decrease dictated by a critical time-scale---the age of the first opposite-sex sexual intercourse (FOSSI). The hypothesis also proposes a modification of the vivo-nergy by the phases of systematic or homeostatic physiology. The hypothesis further postulates that the deviation of the physiology-modified vivo-nergy from the pre-puberty level is deteriorated by the acquired organ-specific pathological conditions. Any deviation of vivo-nergy from the pre-puberty level is hypothesized to be photo-genic, proportionally causing oxidative stress that functions as the physical source of UPE. The age and systematic physiology combined determines the intensity of the physiological photo-genic source confined at the center of the sphere. The acquired (single) pathology sets both the intensity and the off-center position of the (single) pathological photo-genic source. The light emission from a photo-genic source diffuses through the human body that is simplified as a homogeneous spherical domain. The steady-state photon diffusion through the body to the surface is modeled by photon diffusion principles incorporating an extrapolated zero-boundary condition. When the age-related, physiology-commanded, and pathology-controlled modifications of the photo-genetic sources are implemented in the photon diffusion model, the photon fluence rate at the surface of the human-representing spherical domain reveals the patterns of intensity dependence upon age, temporal variation corresponding to systematic physiology, and geometric asymmetry associated with significant asymmetric pathological condition as reported in UPE experimental studies. The hypothesis, as it provides analytical conveniences for quantitative estimation of UPE patterns, may be useful to further model-interpretation of the spatial-temporal characteristics of UPE.

Preprints (www.preprints.org) | NOT PEER-REVIEWED | Posted: 19 October 2018 doi:10.20944/preprints201810.0458.v1

2. Analytical hypothesis of the photo-genic source

A human life of natural course from birth to death can be regarded as experiencing three systematic changes: (1) the initial increase and later stabilization of the body volume-contents, (2) the temporal variation of the biological phases by endocrine and exocrine controls, and (3) the deterioration of the body functions due to acquired pathological conditions. I hypothesize that a human body in the live state is resided with an alternative form of energy named "vivo-nergy", which has a spatially and temporally resolved scalar energy density of $\mathbb{E}_{vivo}(\vec{\chi},t)$ (unit: $J\cdot s^{-1}\cdot cm^{-3}$) at a spatial position $\vec{\chi}$ and a time t. The scalar "vivo-nergy" $\mathbb{E}_{vivo}(\vec{\chi},t)$ takes the following form:

$$\mathbb{E}_{vivo}(\vec{\chi},t)=\mathbb{Z}_{prim}(\vec{\chi},t)\mathbb{H}_{syst}(\vec{\chi},t)\left[1-\mho_{path}(\vec{\chi},t)\cdot\mathbb{N}_{neuro}(\vec{\chi},t)\right], \quad (1)$$

where $\mathbb{Z}_{prim}(\vec{\chi},t)$ (unit: $W\cdot cm^{-3}$) denotes the "primo" state of "vivo-nergy" when descending from birth, $\mathbb{H}_{syst}(\vec{\chi},t)$ (unit: dimensionless) represents the phase of the systematic or homeostatic physiology that is endogenous to a healthy subject, $\mho_{path}(\vec{\chi},t)$ (unit: dimensionless) accounts for the effect of an acquired pathology that is exogenous to an otherwise healthy subject, and $\mathbb{N}_{neuro}(\vec{\chi},t)$ (unit: dimensionless) marks the neuronal networking to the site of the acquired pathology. Additionally, several absolute time-points or characteristic ages of the human life of natural course are symbolized as the following: t_{birth} is the time of birth, t_{death} is the time of death, t_{puber} is the time of puberty so $\tau_{puber}=t_{puber}-t_{birth}$ is the age when puberty starts, and τ_{fossi} is the age of the first opposite-sex sexual intercourse (FOSSI). For a person who commits heterosexual activities at least once in lifetime it is necessary to constrain these time points and ages in the following form: $t_{birth}<t_{puber}<\left(t_{birth}+\tau_{fossi}\right)<t_{death}$. For a person who remains virgin in lifetime, $\tau_{fossi}=(t_{death}-t_{birth})$ will need to be applied. At one's birth, the

Preprints (www.preprints.org) | NOT PEER-REVIEWED | Posted: 19 October 2018 doi:10.20944/preprints201810.0458.v1

following initial conditions are inferred respectively: $\mathbb{Z}_{prim}(\vec{\chi}, t_{birth}) = \mathbb{Z}_0$, $\mathbb{H}_{syst}(\vec{\chi}, t_{birth}) = 1$, $\mathfrak{V}_{path}(\vec{\chi}, t_{birth})$=0, and $\mathbb{N}_{neuro}(\vec{\chi}, t_{birth}) = 1$. The values of these parameters over the life-span of the person denoted by $t \in (t_{birth}, t_{death}]$ is constrained respectively as the following: $\mathbb{Z}_{prim}(\vec{\chi}, t) \in [0, \mathbb{Z}_0]$, $\mathbb{H}_{syst}(\vec{\chi}, t) \in (0,1]$, $\mathfrak{V}_{path}(\vec{\chi}, t) \in [0,1]$ and $\mathbb{N}_{neuro}(\vec{\chi}, t) \in [0,1]$. A pathological condition that is terminal or lethal is represented by $\mathfrak{V}_{path}(\vec{\chi}, t) = 1$. A normal neuronal control of a site of pathological condition is marked by $\mathbb{N}_{neuro}(\vec{\chi}, t) = 1$. The complete loss of the neuronal control of a site of pathological condition is demarcated by $\mathbb{N}_{neuro}(\vec{\chi}, t) = 0$.

For a human life of normal course, it is also reasonable to assume that a life-shortening pathology is acquired after puberty, then the "primo" state of the vivo-nergy $\mathbb{Z}_{prim}(\vec{\chi}, t)$ from birth to puberty would sustain at the initial level of $\mathbb{Z}_0$ set at birth with the only modification incurring due to the systematic or homeostatic physiology $\mathbb{H}_{syst}(\vec{\chi}, t)$. This results in a level-set representation of the vivo-nergy as the following, with the use of the Heaviside or unit step function $u(t)$:

$$\mathbb{E}_{vivo}(\vec{\chi}, t) = \mathbb{Z}_0\left[u(t - t_{birth}) - u\left(t - t_{puber}\right)\right]\mathbb{H}_{syst}(\vec{\chi}, t)$$
$$+\mathbb{Z}_{adol}(\vec{\chi}, t)\left[u\left(t - t_{puber}\right) - u(t - t_{death})\right]\mathbb{H}_{syst}(\vec{\chi}, t)\left[1 - \mathfrak{V}_{path}(\vec{\chi}, t)\mathbb{N}_{neuro}(\vec{\chi}, t)\right] \quad (2)$$

Where $\mathbb{Z}_{adol}(\vec{\chi}, t)$ specifies the "primo" state of the energy counted from t_{puber} as the person enters "adolescence", which is expressed by the following equation:

$$\mathbb{Z}_{adol}(\vec{\chi}, t) = \mathbb{Z}_0\left\{1 - \left[1 - exp\left(-\frac{t - t_{puber}}{\tau_{fossi}}\right)\right]^{\alpha}\right\} \quad (3)$$

where α is a non-zero, positive constant determining the rapidness of the initial deviation of $\mathbb{Z}_{adol}(\vec{\chi}, t)$ from $\mathbb{Z}_0$. I define the deviation of the vivo-nergy from the systematic physiology modified birth state of $\mathbb{Z}_0$ over the lifetime as the following:

Preprints (www.preprints.org) | NOT PEER-REVIEWED | Posted: 19 October 2018 doi:10.20944/preprints201810.0458.v1

$$\Delta\mathbb{E}_{vivo}(\vec{\chi},t) = \mathbb{Z}_0\mathbb{H}_{syst}(\vec{\chi},t) - \mathbb{E}_{vivo}(\vec{\chi},t) \quad (4)$$

By using Eq. (2), it is straightforward to obtain the following:

$$\Delta\mathbb{E}_{vivo}(\vec{\chi},t) = [\mathbb{Z}_0 - \mathbb{Z}_{adol}(\vec{\chi},t)]\mathbb{H}_{syst}(\vec{\chi},t)\left[u\left(t-t_{puber}\right) - u(t-t_{death})\right]$$
$$+\mathbb{Z}_{adol}(\vec{\chi},t)\mathbb{H}_{syst}(\vec{\chi},t)\mho_{path}(\vec{\chi},t)\mathbb{N}_{neuro}(\vec{\chi},t)\left[u\left(t-t_{puber}\right) - u(t-t_{death})\right] \quad (5)$$

Two entities of differential properties are introduced as shown respectively in the following:

$$\Delta\mathbb{Z}_{adol}(\vec{\chi},t) = \mathbb{Z}_o\left[1 - exp\left(-\frac{t-t_{puber}}{\tau_{fossi}}\right)\right]^{\alpha}\mathbb{H}_{syst}(\vec{\chi},t) \quad (6)$$

$$\Delta\mho_{path}(\vec{\chi},t) = \mathbb{Z}_0\left\{1 - \left[1 - exp\left(-\frac{t-t_{puber}}{\tau_{fossi}}\right)\right]^{\alpha}\right\}\mathbb{H}_{syst}(\vec{\chi},t)\mho_{path}(\vec{\chi},t)\mathbb{N}_{neuro}(\vec{\chi},t) \quad (7)$$

Equation (5) then becomes

$$\Delta\mathbb{E}_{vivo}(\vec{\chi},t) = \{\Delta\mathbb{Z}_{adol}(\vec{\chi},t) + \Delta\mho_{path}(\vec{\chi},t)\}\left[u\left(t-t_{puber}\right) - u(t-t_{death})\right] \quad (8)$$

where the first "differential" component $\Delta\mathbb{Z}_{adol}$ as specified by Eq. (6) denotes the deviation of the "vivo-nergy" from the "primo" state as a result of normal biological development, and the second "differential" component $\Delta\mho_{path}$ as specified by Eq. (7) represents the further deviation of the "vivo-nergy" from the level normal to an age due to acquired pathology.

The Eq. (8) by referring to Eqs. (6) and (7) can infer the age-dependency of $\Delta\mathbb{E}_{vivo}$ by setting $\mathbb{H}_{syst}(\vec{\chi},t)$=1 and $\mho_{path}(\vec{\chi},t) = 0$, the effect of systematic physiology over a time period by setting $\mho_{path}(\vec{\chi},t) = 0$, and the outcome of acquired pathology at a given time point by setting $\mathbb{H}_{syst}(\vec{\chi},t)$=1. The hypothetic changes of the "vivo-nergy" over the life span of a human being are illustrated in **Figure 1**, where (A) marks the initial level of "vivo-nergy" set at birth, (B) specifies the decrease of "vivo-nergy" starting at puberty as a result of growth and aging, (C) represents the deviation of "vivo-nergy" from the age-related level due to modulation by

Preprints (www.preprints.org) | NOT PEER-REVIEWED | Posted: 19 October 2018 doi:10.20944/preprints201810.0458.v1

systematic physiology, and (D) manifests the degradation of "vivo-nergy" from the healthy level for an age when caused by acquired pathology.

The deviation of the "vivo-nergy" from the "primo" state is projected to become photo-genic through the oxidative bio-chemical pathways that produce free radicals [34, 35]. Integration of the spatially resolved differential "vivo-nergy" represented by Eqs. (6) and (8) over the body volume gives rise to the following two spectrally and temporally resolved photo-genic intensity terms:

$$\mathbb{S}_{syst}(\lambda, t) = \varrho_{syst}(\lambda, t) \iiint \Delta\mathbb{Z}_{adol}(\vec{\chi}, t)\, d\vec{\chi}^3 \tag{9}$$

$$\mathbb{S}_{path}(\lambda, t) = \eth_{path}(\lambda, t) \iiint \Delta\mho_{path}(\vec{\chi}, t)\, d\vec{\chi}^3 \tag{10}$$

where $\varrho_{syst}(\lambda, t)$ (unit: dimensionless) is the spectrally and temporally resolved physiological-photogenic factor, and $\eth_{path}(\lambda, t)$ (unit: dimensionless) is the spectrally and temporally resolved pathological-photogenic factor. The human body is simplified as a volume of spherical domain of radius R_0 as shown in **Figure 2**. The physiological photo-genic source $\mathbb{S}_{syst}$ (unit: W) is set at the center of the spherical domain, whereas the pathological photo-genic source $\mathbb{S}_{path}$ (unit: W) that is associated with a single serious organ-specific pathology could be positioned at any distance R_{path} to the center. The spherical coordinates of the pathological photo-genic source $\mathbb{S}_{path}$ are set as $(\mathrm{R}_{path}, \theta', \phi')$, or for convenience of visualization at the 3 o'clock position with respect to the center of the spherical body in assessing the effect on specifically the left-right symmetry by this single pathological photo-genic source. The spectral and temporal dependences of the photo-genic sources $\mathbb{S}_{syst}$ and $\mathbb{S}_{path}$ are not considered in the following, i.e. $\varrho_{syst}(\lambda, t) = \varrho_{syst} = constant$, $\eth_{path}(\lambda, t) = \eth_{path} = constant$, thus $\mathbb{S}_{syst}$ and $\mathbb{S}_{path}$ are steady-state sources that will facilitate analysis of the simplest steady-state photon propagation in the body volume.

Preprints (www.preprints.org) | NOT PEER-REVIEWED | Posted: 19 October 2018 doi:10.20944/preprints201810.0458.v1

3. Photon diffusion causing surface photon emission

With the placement of a steady-state photo-genic source in the spherical tissue domain representing the human body, the steady-state propagation of the photon in the spherical domain that is several orders greater than the photon scattering path-length in a biological tissue can thus be modeled by the diffusion approximation to the radiative transfer [36]. The human body is treated as a globally homogeneous diffusive medium containing localized steady-state spatially impulsive photo-genic sources. The diffusive tissue medium is characterized by the following properties: absorption coefficient $\boldsymbol{\mu_a}$ [unit: cm^{-1}], reduced scattering coefficient $\boldsymbol{\mu_s'}$ [unit: cm^{-1}], diffusion coefficient $\boldsymbol{D = 1/[3(\mu_a + \mu_s')]}$ [unit: cm], and effective attenuation coefficient $\boldsymbol{\mu_{eff} = \sqrt{\mu_a/D} = \sqrt{3\mu_a\mu_s'}}$ [unit: cm^{-1}]. For a field or detection position at $\vec{\boldsymbol{\chi}} = (\boldsymbol{r}, \boldsymbol{\theta}, \boldsymbol{\varphi})$ within the globally homogeneous tissue domain including that on the tissue-air boundary, the steady-state photon fluence rate $\Psi(\vec{\chi})$ (unit: s^{-1}cm^{-2}) satisfies the following equation [37]:

$$\nabla^2\Psi(\vec{\chi}) - \frac{\mu_a}{D}\Psi(\vec{\chi}) = -\frac{S(\vec{\chi})}{D} \tag{11}$$

where $S(\vec{\chi})$ is a source term, which is also subject to a boundary condition. For an infinite homogeneous medium containing a steady-state point source at $\vec{\chi}'$ with an intensity S as is represented by $S \cdot \delta(\vec{\chi}')$, Eq. (11) has the well-known Green's function solution of [38]

$$\Psi(\vec{\chi}, \vec{\chi}') = \frac{S}{4\pi D}\frac{1}{|\vec{\chi} - \vec{\chi}'|}exp\left(-\mu_{eff}|\vec{\chi} - \vec{\chi}'|\right) \tag{12}$$

The solution Eq. (12) can also be written in the following Eigen function expansion [39]:

$$\Psi(\vec{\chi}, \vec{\chi}') = \frac{S}{D}\left(\mu_{eff}\right)\sum_{l=0}^{\infty}\left[i_l\left(\mu_{eff}r_<\right)\cdot k_l\left(\mu_{eff}r_>\right)\right]\sum_{m=-l}^{l}[Y_{lm}^*(\theta', \phi')\cdot Y_{lm}(\theta, \phi)] \tag{13}$$

Preprints (www.preprints.org) | NOT PEER-REVIEWED | Posted: 19 October 2018 doi:10.20944/preprints201810.0458.v1

where i_l and k_l are respectively the l-th order modified spherical Bessel function of the first and the second kinds, $r_<$ and $r_>$ are respectively the smaller and greater radial coordinates of the source and detector, and Y_{lm} is the spherical harmonics function.

With regards to how the photon fluence rate is affected by the tissue-air boundary, it has been established that the photon fluence rate does not become zero at a field position immediately beyond the tissue boundary; instead, a more accurate treatment of extrapolated zero-boundary condition sets zero the photon fluence rate at a distance away from the tissue boundary-------the so called extrapolated boundary [40]. The Figure 2 with the implementation of the extrapolated boundary is illustrated in **Figure 3**. A field point $\vec{\chi}$ on or beyond the spherical tissue boundary locates at (r, θ, φ) with $r \geq R_0$. The application of the extrapolated zero-boundary condition to the photon fluence rate associated with any source within the tissue medium is satisfied by introducing an "image" of the source with respect to the extrapolated boundary that is co-centric with and at a radial distance of $R_b = 2AD$ outward from the physical boundary [39] where $A = (1 + \xi)/(1 - \xi)$, $\xi = -1.440n^{-2} + 0.710n^{-1} + 0.668 + 0.0636n$, and n is the refractive index of the air-bounding tissue. As the composite photon fluence rate resulted from both the physical source in the tissue medium and the image of it becomes zero at the extrapolated boundary, the composite positive photon fluence rate elsewhere resulted from the same two sources of one being physical and the other being imaginary thus become the solution in the associated physical space within the body volume or beyond the boundary, according to the uniqueness theorem governing electromagnetism.

For the pathological photo-genic source $\mathbb{S}_{path}$ located off-center at $(R_{path}, \theta', \phi')$, the geometric symmetry determines that the image of it with respect to the extrapolated boundary must locate along the same radial direction of it. The source $\mathbb{S}_{path}$ and its image with respect to the

Preprints (www.preprints.org) | NOT PEER-REVIEWED | Posted: 19 October 2018 doi:10.20944/preprints201810.0458.v1

extrapolated boundary thus collectively set zero the photon fluence rate on the extrapolated boundary. Based on Eq. (13), the photon fluence rate associated with the pathological photo-genic source $\mathbb{S}_{path}$ and evaluating on the extrapolated boundary, for which the source locates at $r_< = R_{path}$ and the field point locates at $r_> = R_0 + R_b$, is

$$\Psi_{path}\big|_{extra} = \mathbb{S}_{path}\frac{1}{D}(\mu_{eff})\sum_{l=0}^{\infty} i_l[\mu_{eff}\cdot(R_{path})]\cdot k_l[\mu_{eff}(R_0+R_b)]$$

$$\sum_{m=-l}^{l} Y_{lm}^*(\theta',\phi')Y_{lm}(\theta,\phi) \qquad (14)$$

where the notation "$_{left}\big|_{right}$" indicates evaluating the "left" as the source on the "right" as the field position. Note that that any "l"th order (or moment) of the pathological photo-genic source has the same intensity of $\mathbb{S}_{path}$. Similarly, the photon fluence rate associated with the image of the pathological photo-genic source and evaluating on the extrapolated boundary, for which the source now locates at a radial position of a to-be-determined $r_>$ and the detector locates at $r_< = R_0 + R_b$, is

$$\Psi_{path}^{imag}\big|_{extra} = \frac{1}{D}(\mu_{eff})\sum_{l=0}^{\infty} S_l^*\cdot i_l[\mu_{eff}(R_0+R_b)]\cdot k_l[\mu_{eff}r_>]$$

$$\sum_{m=-l}^{l} Y_{lm}^*(\theta',\phi')Y_{lm}(\theta,\phi) \qquad (15)$$

where the S_l^* terms is different for different "l" (or moment). Based on the essence of "image-source" [35, 36], the two unknown terms S_l^* and $r_>$ associated with the l-th order (or moment) "image" source (the k_l component) can be expressed by a single unknown term S_l associated with the same order (or moment) of the actual pathological photo-genic source $\mathbb{S}_{path}$ located within the tissue at (R_{path},θ',ϕ') (the i_l component), as the following:

Preprints (www.preprints.org) | NOT PEER-REVIEWED | Posted: 19 October 2018 doi:10.20944/preprints201810.0458.v1

$$S_l^* \cdot k_l[\mu_{eff} r_>] = S_l \cdot i_l[\mu_{eff}(R_{path})] \tag{16}$$

Applying the extrapolated zero-boundary condition of $\Psi_{path}\big|_{extra} + \Psi_{path}^{imag}\big|_{extra} = 0$ leads to

$$S_l = -\mathbb{S}_{path} \frac{k_l[\mu_{eff}(R_0+R_b)]}{i_l[\mu_{eff}(R_0+R_b)]} \quad l = 0,1,2,\ldots \tag{17}$$

Now for the photon fluence rate associated with the pathological photo-genic source at $(R_{path}, \theta', \phi')$, but evaluating at a field point between the body boundary and the extrapolated boundary, the source still locates at $r_< = R_{path}$ but the detector or the field point locates at $r_> = R_0 + \Delta r$, where $\Delta r \in [0, R_b]$. For the photon fluence rate associated with the image of the pathological photo-genetic source and also evaluating at a field point between the body boundary and the extrapolated boundary, the field point now locates at $r_< = R_0 + \Delta r$ and the source terms are known through Eqs. (16) and (17). Collectively the composite photon fluence rate originating from a pathological photo-genic source at $(R_{path}, \theta', \phi')$ and sensed by a detector or field point at $(R_0 + \Delta r\,, \theta, \phi)$ between the body boundary and the extrapolated boundary becomes:

$$\Psi_{path} = \Psi_{path}\big|_{field} + \Psi_{path}^{imag}\big|_{field}$$

$$= \frac{\mathbb{S}_{path}}{D}(\mu_{eff}) \sum_{l=0}^{\infty} i_l[\mu_{eff}(R_{path})] \cdot k_l[\mu_{eff}(R_0 + \Delta r)] \sum_{m=-l}^{l} Y_{lm}^*(\theta', \phi') Y_{lm}(\theta, \phi)$$

$$- \frac{\mathbb{S}_{path}}{D}(\mu_{eff}) \sum_{l=0}^{\infty} \cdot i_l[\mu_{eff}(R_0 + \Delta r)] i_l[\mu_{eff}(R_{path})]$$

$$\cdot \frac{k_l[\mu_{eff}(R_0 + R_b)]}{i_l[\mu_{eff}(R_0 + R_b)]} \sum_{m=-l}^{l} Y_{lm}^*(\theta', \phi') Y_{lm}(\theta, \phi)$$

$$= \frac{\mathbb{S}_{path}}{D}(\mu_{eff}) \sum_{l=0}^{\infty} i_l[\mu_{eff}(R_{path})] \cdot k_l[\mu_{eff}(R_0 + \Delta r)] \sum_{m=-l}^{l} Y_{lm}^*(\theta', \phi') Y_{lm}(\theta, \phi)$$

Preprints (www.preprints.org) | NOT PEER-REVIEWED | Posted: 19 October 2018 doi:10.20944/preprints201810.0458.v1

$$\left\{1-\frac{i_l[\mu_{eff}(R_0+\Delta r)]}{k_l[\mu_{eff}(R_0+\Delta r)]}\frac{k_l[\mu_{eff}(R_0+R_b)]}{i_l[\mu_{eff}(R_0+R_b)]}\right\} \tag{18}$$

Equation (18) contains two parts: the "1" in the bracket represents the infinite-medium contribution to the photon fluence rate by the pathological photo-genic source $\mathbb{S}_{path}$ that can be expressed by the simple form of Eq. (12); and the other term in the bracket scales the infinite-medium contribution to the photon fluence rate by the image of the pathological photo-genic source $\mathbb{S}_{path}$ with respect to the former one. By using some analytics of the modified spherical Bessel function and Eq. (12), Eq. (18) is converted to the following form [39]

$$\Psi_{path}=\frac{\mathbb{S}_{path}}{4\pi D}\frac{1}{l_{path}}exp\left(-\mu_{eff}l_{path}\right)\left\{1-\frac{I_{l+1/2}[\mu_{eff}(R_0+\Delta r)]}{K_{l+1/2}[\mu_{eff}(R_0+\Delta r)]}\frac{K_{l+1/2}[\mu_{eff}(R_0+R_b)]}{I_{l+1/2}[\mu_{eff}(R_0+R_b)]}\right\} \tag{19}$$

where $I_{l+\frac{1}{2}}$ and $K_{l+\frac{1}{2}}$ are respectively the $\left(l+\frac{1}{2}\right)$-th order modified Bessel function of the first and the second kinds. For a human body simplified as a spherical domain, it is easy to have an R_0 (i.e., 10cm) that is substantially greater than 10 times of $1/\mu_{eff}$ to have the second term in the bracket of Eq. (19) approximated by

$$\frac{I_{l+1/2}[\mu_{eff}(R_0+\Delta r)]}{K_{l+1/2}[\mu_{eff}(R_0+\Delta r)]}\frac{K_{l+1/2}[\mu_{eff}(R_0+R_b)]}{I_{l+1/2}[\mu_{eff}(R_0+R_b)]}=exp\left[-2\mu_{eff}(R_b-\Delta r)\right] \tag{20}$$

Thus Eq. (19) will be changed to a trivial form of

$$\Psi_{path}=\frac{\mathbb{S}_{path}}{4\pi D}\frac{1}{l_{path}}exp\left(-\mu_{eff}l_{path}\right)\{1-exp\left[-2\mu_{eff}(R_b-\Delta r)\right]\} \tag{21}$$

Equation (21) that is associated with the pathological photo-genic source of $\mathbb{S}_{path}$ pedestrianly satisfies the condition of producing zero composite photon fluence rate at the extrapolated boundary whereupon $\Delta r=R_b$. Equation (21) also determines that the photon fluence rate associated with the pathological photo-genic source of $\mathbb{S}_{path}$ decreases monotonically from the body boundary to the extrapolated boundary. One can find that, a hypothetical movement of

Preprints (www.preprints.org) | NOT PEER-REVIEWED | Posted: 19 October 2018 doi:10.20944/preprints201810.0458.v1

the photo-genic source like the pathological one $\mathbb{S}_{path}$from $(R_{path}, \theta', \phi')$ toward the center of the spherical domain can maintain the boundary-resulted composite photon fluence rate as the form of Eq. (21), with the length dimension l_{path} varying according to the position of the photo-genic source. The hypothetical experiment infers that the boundary-resulted composite photon fluence rate at a field point at $(R_0 + \Delta r, \theta, \varphi)$ in association with a physiological photo-genic source $\mathbb{S}_{syst}$ located at the center of the spherical domain can be represented as the following:

$$\Psi_{syst} = \frac{\mathbb{S}_{syst}}{4\pi D} \frac{1}{l_{syst}} exp\left(-\mu_{eff} l_{syst}\right)\left\{1 - exp\left[-2\mu_{eff}(R_b - \Delta r)\right]\right\} \quad (22)$$

where l_{syst} is the distance from the physiological photo-genic source to the field point. When both the physiological patho-genic source $\mathbb{S}_{syst}$ and the pathological photo-genic source $\mathbb{S}_{path}$ are considered as the origin of the photon emission causing UPE photon distribution beyond the spherical boundary, the composite photon fluence rate at a field point $(R_0 + \Delta r, \theta, \varphi)$ is thus the combination of the respective photon flounce rates of Eqs. (21) and (22), as the following:

$$\Psi_{UPE} = \frac{1}{4\pi D}\left[\mathbb{S}_{syst} \frac{1}{l_{syst}} exp\left(-\mu_{eff} l_{syst}\right) + \mathbb{S}_{path} \frac{1}{l_{path}} exp\left(-\mu_{eff} l_{path}\right)\right] \left\{1 - exp\left[-2\mu_{eff}(R_b - \Delta r)\right]\right\} \quad (23)$$

4. Numerical evaluation of the superficial photon fluence rate of the spherical domain

Equation (23) is implemented numerically to assess the patterns of photon fluence rate presenting at or beyond the air-interfacing boundary of the human-representing spherical homogeneous tissue domain in association with the physiological photo-genic source $\mathbb{S}_{syst}$ alone or the addition of the pathological photo-genic source $\mathbb{S}_{path}$. The distribution of the photon fluence rate across the surface of the human-representing spherical domain and expanding to the extrapolated boundary is exemplified in **Figure 4**. The tissue medium used for all numerical evaluations in this section is

Preprints (www.preprints.org) | NOT PEER-REVIEWED | Posted: 19 October 2018 doi:10.20944/preprints201810.0458.v1

specified with the following dimensional and optical properties: a radius of $\boldsymbol{R}_0 = 10cm$, an absorption coefficient of $\boldsymbol{\mu_a} = 0.1$ cm^{-1}, a reduced scattering coefficient of $\boldsymbol{\mu_s'} = 10$ cm^{-1}, and a refractive index of n=1.4. The tissue optical properties result in a distance of $\boldsymbol{R}_b = 0.11cm$ of the extrapolated boundary from the tissue boundary, which is only 1.1% of the radius of the spherical domain. When the tissue medium represented by the spherical domain contains only the centered physiological photo-genic source $\mathbb{S}_{syst}$, the photon fluence rate on the entire spherical boundary has to be uniform, and the photon fluence rate will decrease from the tissue boundary to become zero at the extrapolated boundary. The degradation of the photon fluence rate from the tissue boundary to the extrapolated boundary over an entire azimuthal or elevational circle will appear as a thin circular strip of 0.11cm thick around the spherical tissue domain. To better visualize this thin circular strip of the photon fluence rate around the spherical tissue domain in Figure 4, the evaluation of the Eq. (23) over space beyond the tissue boundary is conducted over a radial distance of 10 times of $\boldsymbol{R}_b$, i.e. a 1.1cm distance from the tissue boundary as the strip of lower color value outside the dashed circle demarcating the spherical tissue boundary. In obtaining Fig. 4, the following additional parameters are necessary: $\mathbb{S}_{syst} = 0.01\mu W$ and $\mathbb{S}_{path} = 0$. The uniform photon fluence rate across the spherical tissue domain represents the 2-dimentional projection of the photon fluence rate measured on the surface of the spherical tissue domain as is the case for measurement/imaging using a planar pixelated photon detection device. The photon fluence rate projected on the surface of a spherical tissue domain of the associated optical properties with a 10cm radius and a 0.01μW source at the center is at the level of $1\times 10^{-17} W \cdot cm^{-2}$ (corresponding to 25 counts of 500nm photons per second per cm^2), and drops to zero at the extrapolated boundary that in actual scale is just about 0.11cm away from the tissue boundary of the specified optical properties.

Preprints (www.preprints.org) | NOT PEER-REVIEWED | Posted: 19 October 2018 doi:10.20944/preprints201810.0458.v1

In the following sections, the numerical implementations of Eq. (23) are configured in 3 cases of the photo-genetic sources to demonstrate respectively the patterns of age-dependency, physiological variation, and pathological asymmetry of the photon-fluence rate at the surface of the spherical domain. It is noted that the temporal variation is assessed via relative changes of the photon fluence rate evaluated at the same spatial location. Therefore when the photon fluence rate is to be evaluated at one position to assess the temporal changes at any durations, the position of the field point is set at the boundary of the spherical tissue boundary and at 3 o'clock position, and the resulted photon fluence rate is scaled across the board to compare against a few literature data that are reproduced with the publishers' permissions.

4.1 Age dependency

The age dependency and gender difference of the photon fluence rate at the boundary of the spherical tissue domain is simulated by removing $\mathbb{S}_{path}$ and setting the following parameters: the puberty age τ_{puber} of male is 13, the puberty age τ_{puber} of female is 11, the FOSSI age τ_{fossi} of both male and female is 20, the power factor determining the rapidness of the age-dependency is $\alpha = 2$, and a life spans 75 years. The male weight is assumed to be 40% greater than the female weight at the same age, leading to 40% stronger intensity of the physiological photo-genic source $\mathbb{S}_{syst}$ for male than female at otherwise identical setting of the parameters. A literature report showing the dependency of UPE photon count on age and the difference of UPE photon count between male and female is reproduced with permission from the publisher [27] as shown in **Figure 5**(A). In (A) there is a smaller down-ward solid-framed arrow pointing to an age group of 11-14 of both male and female, at which the UPE photon count started to increase noticeably. That age group is projected to indicate puberty. In (A) there is a larger upward dash-framed arrow

Preprints (www.preprints.org) | NOT PEER-REVIEWED | Posted: 19 October 2018 doi:10.20944/preprints201810.0458.v1

pointing to an age group of 41-50 of the female that may be interpreted as indicating menopause. That menopause-inferring change is not included in the numerical model analysis *per se*. The numerical results as specified heretofore are plotted in Figure 5(B) with the the assumption of the photon fluence rate has a baseline count at the level of the literature report. The patterns regarding how the photon fluence rates change over the age and how different the chances are between the male and female resemble the trends reported.

4.2 Diurnal variation

The variation of the photon fluence rate revealed at the boundary of the spherical tissue domain as a function of short-term homeostatic changes is simulated by removing $\mathbb{S}_{path}$ and setting the $\mathbb{H}_{syst}$ to change periodically. A known diurnal variation of UPE photon count is adopted from an open-access publication [41] as shown in **Figure 6**(A). The UPE intensity revealed a trough in the later afternoon and a peak in early morning. That diurnal variation over a range of approximately 90-110% of the mid-line level can be directly attributed to the circadian cycle. The circadian cycle is thus implemented into the intensity of physiological photo-genic source in Eq. (23) by setting $\mathbb{H}_{syst}(\vec{\chi}, t) = 0.9 + 0.1cos\left(\frac{\pi}{4}t - \frac{\pi}{2}\right)$. This circadian-like systematric change results in $\mathbb{H}_{syst}(\vec{\chi}, t)$ to vary between 1 and 0.8. The resulted photon fluence rate as shown in (b) varies at a cycle close to that manifested by the more noisy presentation of (A).

4.3. Spatial asymmetry associated with asymmetric pathological conditions

The spatial asymmetry of surface photon fluence rate can be induced by placing a pathological photo-genic source off-center in the spherical domain. Such a demonstration is given in Figure 7

Preprints (www.preprints.org) | NOT PEER-REVIEWED | Posted: 19 October 2018 doi:10.20944/preprints201810.0458.v1

in referencing the asymmetric UPE intensity that became aggregated as the tumor-load at the right axillary of a breast cancer mouse model increased [16]. The tumor volume is modeled as increasing exponentially [42]. The tumor volumes of respectively less than 0.5cm in diameter, between 1cm and 1.5cm in diameter, and greater than 1.5m in diameter as specified on panel (A) are modeled as $\exp(\frac{1}{1.5})$, $\exp(\frac{2}{1.5})$, and $\exp(\frac{3}{1.5})$ as plotted on the panel (B). The resulted numerical value of the tumor size is scaled down to 1% and used as the intensity of the pathological photo-genic source $\mathbb{S}_{path}$ that is placed at 1cm off the center at the right-lateral aspect and 1cm off center at the right anterior aspect, as illustrated in the left column of panel (C). In comparison, the centered physiological photo-genic source $\mathbb{S}_{syst}$ is set to have an intensity 1. The intensity ratios of the centered physiological photo-genic source $\mathbb{S}_{syst}$ over the slightly off-centered pathological photo-genic source $\mathbb{S}_{path}$ for the three sizes of the tumor load are thus respectively 1 vs 0.0195, 1 vs 0.0379, and 1 vs 0.739. The resulted photon fluence rate over the surface of the spherical tissue domain that is projected to the middle cross-section and surrounded by a thin strip of the space beyond the tissue boundary is presented in the middle column of panel (C). The left-right asymmetry of the surface photon fluence rate becomes pronounced as the localized pathological photo-genic source increases in the intensity. The 1-dimentional profile along the diameter crossing the 9 o'clock position to the 3 o'clock position of the 2-dimensional photon fluence rate map of the middle column of panel (C) is given at the right column. For a baseline arbitrary photon fluence rate of 300 over the tissue domain that is least affected by the pathological photo-genic source, the global change of the maximal photon fluence rate in the right lateral region of the side of the pathological photo-genic source increases from the baseline level to approximately 600. The pattern of the photon fluence rate at the right lateral side is similar to that of the UPE pattern shown

Preprints (www.preprints.org) | NOT PEER-REVIEWED | Posted: 19 October 2018 doi:10.20944/preprints201810.0458.v1

on panel (A). Meanwhile, the maximal photon fluencer rate in the contra-lateral aspect of the pathological photo-genic source has increased slightly from the baseline, as the left-right difference becomes pronounced. This pattern of slight chance on the contra-lateral normal side can also be traced back to the UPE pattern shown on panel (A).

5. Discussions

This work is intended to provide a quantitative model-based interpretation of a few patterns of UPE that are presented as superficial patterns that indicate the effect of age, the systematic physiology, and localized pathological conditions. An apparent limitation of this model is the unknown value of the photo-genetic factor for converting the hypothetical deviation of the vivo-nergy from an optimal primo state to a physical source of light emission. The photo-genetic factor may not be specified unless the new form of the energy residency as “vivo-nergy” can be justified. Another limitation is the modeling of the human tissue volume as a spherical domain, even though it is obviously more accurate than the most commonly treated semi-infinite tissue domain that is friendly to analytical treatment. The advantage of a spherical tissue domain is the involvement of only one boundary as the geometry involves essentially a radial dependency. A more practical geometry of representing human tissue volume in terms of photon propagation may be a cylindrical domain of finite-length, within which the similar photon diffusion approach can be applied. Applying the photon diffusion approach to a finite length cylindrical tissue domain will require considering boundary at two orientations, one is along the radial dimension and the other is along the polar aspect. That treatment may reveal that the strips of photon emission at the cranial and caudal aspects of the human body differ from the strips of photon emission at lateral aspects of the human body [43].

 doi:10.20944/preprints201810.0458.v1

In this work, the physiological photo-genic source is localized at the center of the human tissue domain, in consideration of the systematic influence of any homeostatic cause. The localization of the pathological photo-genic causes to only one off-center source is rather arbitrary. But the results associated with a single off-center pathological photo-genic source can be conveniently expanded to the case of having multiple pathological conditions that each demands an individual photo-genic source. In such cases, multiple pathological photo-genic sources of different intensities can be localized at different positions that potentially represent their site-specific anatomy, and the spatially resolved photon fluence rates resulted from those multiple pathological photo-genic sources can be combined in a linear format to inform the composite photon fluence rate at the surface. For a more complicated tissue geometry, the computation of the surface photon fluence rate can also be conducted by using numerical procedures such as finite-element methods (FEM) [44] for solving photon diffusion problems. Implementing numerical methods such as FEM may also allow addressing complicated pathological photon-genic causes that are better represented by a source distributed over a continuous tissue volume.

The pathological condition has been linked with neuronal control in deriving the photo-genic source term in this model. A site of pathological condition that has lost the neural control will lead to less deviation from the primo state of the vivo-nergy, thus smaller intensity of the photon-genic source. A smaller photon-genic source will result in smaller superficial photon fluence rate at the side of the pathological condition, or equivalently higher superficial photon fluence rate at the contra-lateral side. This arrangement of the neuronal control will make the model output in consistent with the observation of lower UPE at the hand of hemiparesis when compared to the normal contra-lateral hand [32]. The validity of defining the photo-genic effect of neuronal control for modeling superficial patterns of UPE will be subject to further testing.

 doi:10.20944/preprints201810.0458.v1

The temporal changes of the superficial photon fluence rate have been estimated in this work for a single case of diurnal-like variation over a short 24-hours period. The approach is however easily applicable to modeling temporal changes over a time scale much different from a day-long period. Evaluating if the temporal changes of the superficial photon fluence rate over a longer-than-day scale represent the temporal changes of UPE over the similar time scale will require the precise knowledge of how the homeostatic changes over the same time scale may alter the intensity of the physiological photo-genic source. The convenience of this model work for estimating the temporal changes of the superficial photon fluence rate, on the other hand, may facilitate modeling of the temporal pattern of UPE under short stimulation of UPE causes. This will require treating the photon diffusion problem as a temporal problem, not the steady-state problem as is simplified in this part of the work that explores the feasibility of model-based approach to superficial patterns of UPE.

6. Conclusions

In conclusion, I present an analytical framework of hypothesis for the initial objective of modeling a few superficial presentations of UPE of human, including the systematic dependency on age, the diurnal variation, and the geometric asymmetry associated with serious asymmetrical pathological conditions. The hypothesis assumes a new form of energy state, termed vivo-nergy, which resides only in metabolically active organisms that are also under neuronal control. The hypothesis projects a decrease of the vivo-nergy in human during growth beyond puberty, with the rate of decrease dictated by a critical time-scale---the age of the first opposite-sex sexual intercourse (FOSSI). The hypothesis also proposes a modification of the vivo-nergy by the phases of systematic or homeostatic physiology. The hypothesis further postulates that the deviation of the physiology-modified vivo-nergy from the pre-puberty level is deteriorated by acquired organ-

Preprints (www.preprints.org) | NOT PEER-REVIEWED | Posted: 19 October 2018 doi:10.20944/preprints201810.0458.v1

specific pathological conditions. Any reduction of vivo-nergy from the pre-puberty level is hypothesized to proportionally cause oxidative stress that functions as the physical source of UPE. The resulted steady-state diffusion of the photon emitted from a photo-genic source of UPE in a human geometry simplified as a homogeneous spherical domain is modeled by photon diffusion principles incorporating an extrapolated zero-boundary condition. The age and systematic physiology combined determines the intensity of the centered physiological photo-genic source. The acquired (single) pathology sets both the intensity and the off-center position of the (single) pathological photo-genic source. When the photo-genetic sources are implemented in the photon diffusion model, the photon fluence rate at the surface of the simplified human-representing spherical domain reveals the age-dependency, homeostatic variation, and pathology-induced asymmetry of UPE. The hypothesis, amay be useful to further model-based interpretation of the spatial-temporal characteristics of UPE.

Figure Captions:

Figure 1. (A)The vivo-nergy bestowed on a person at birth. (B) The decrease of the "vivo-nergy" of a healthy person due to aging. (C) The modulation of the "vivo-nergy" of a healthy person by systematic physiology. (D) The degradation of the "vivo-nergy" of a person from the healthy level by acquired pathology.

Figure 2. The human body is simplified as a spherical geometry with a radius R_0. The physiological photo-genic source $\mathbb{S}_{syst}$ is set at the center of the spherical domain, or with the spherical coordinates of (0,0,0). The pathological photo-genetic source $\mathbb{S}_{path}$ is positioned at 3

Preprints (www.preprints.org) | NOT PEER-REVIEWED | Posted: 19 October 2018 doi:10.20944/preprints201810.0458.v1

o'clock position with respect to the spherical center, at $(R_{path}, 0, 0)$. The distance of any position (R_0, θ, ϕ) on or off the spherical surface to the pathological source $\mathbb{S}_{path}$ is denoted as l_{path}.

Figure 3. The human body containing a physiological photo-genic source of $\mathbb{S}_{syst}$ at the center of the spherical domain, and a single pathological photo-genetic source $\mathbb{S}_{path}$ at $(R_{path}, 0, 0)$. The photon emitted by a photo-genic source diffuses in the human body and encounters a refractive index discontinuity at the body boundary. The effect of the tissue-air boundary is accounted for by setting the photon fluence rate at an imaginary boundary extrapolated from the physical boundary at a distance of R_b. The image of the single pathological photo-genetic source $\mathbb{S}_{path}$ locates at the radial direction of $\mathbb{S}_{path}$ due to the obvious symmetry. The intensity of the image of the single pathological photo-genetic source $\mathbb{S}_{path}$ may become - $\mathbb{S}_{path}$ in the case of the tissue becoming semi-infinite domain.

Figure 4. Example of the distribution of the photon fluence rate across the surface of the human-representing spherical domain and expanding to the extrapolated boundary. The degradation of the photon fluence rate from the tissue boundary to the extrapolated boundary over an entire azimuthal or elevational circle illustrates as a thin circular strip around the spherical tissue domain.

Figure 5. The age dependency and gender difference of the UPE demonstrated in a literature study [x] in (A) and the simulated photon fluence rate at the boundary of the spherical tissue domain in (B). (A) there is a smaller down-ward solid-framed arrow pointing to an age group of 11-14 of both male and female, at which the UPE photon count started to increase noticeably. That age

Preprints (www.preprints.org) | NOT PEER-REVIEWED | Posted: 19 October 2018 doi:10.20944/preprints201810.0458.v1

group is projected to indicate puberty. In (A) there is a larger upward dash-framed arrow pointing to an age group of 41-50 of the female that may be interpreted as indicating menopause.

Figure 6. A literature report showing the diurnal variation of UPE photon count is adopted from an open-access publication [41] as shown in (A). The UPE intensity revealed a trough at in later afternoon and a peak in early morning. That diurnal variation over a range of approximately 90-110% of the mid-line level can be directly associated with the circadian cycle. The variation of the photon fluence rate revealed at the boundary of the spherical tissue domain as a function of short-term homeostatic changes is simulated by removing $\mathbb{S}_{path}$ and setting the $\mathbb{H}_{syst}$ to change periodically. The circadian cycle is implemented into the intensity of physiological photo-genic source in Eq. (21) by setting $\mathbb{H}_{syst}(\vec{\chi}, t) = 0.9 + 0.1cos\left(\frac{\pi}{4}t - \frac{\pi}{2}\right)$.

Figure 7. (A) the asymmetric UPE intensity that became aggregated as the tumor-load at the right axillary of a breast cancer mouse model increased [16]. The tumor volumes of respectively less than 0.5cm in diameter, between 1cm and 1.5cm in diameter, and greater than 1.5m in diameter as specified on panel (A) are scaled as $\exp(\frac{1}{1.5})$, $\exp(\frac{2}{1.5})$, and $\exp(\frac{3}{1.5})$ as plotted on the panel (B). The resulted numerical value of the tumor size is scaled to 1% and used as the intensity of the pathological photo-genic source $\mathbb{S}_{path}$ that is placed at 1cm off the center at the right-lateral aspect and 1cm off center at the right anterior aspect, as illustrated in the left column of panel (C). The resulted photon fluence rate over the surface of the spherical tissue domain that is projected to the middle cross-section and surrounded by a thin strip of the space beyond the tissue boundary is presented in the middle column of panel (C). The 1-dimentional profile along the diameter crossing

 doi:10.20944/preprints201810.0458.v1

the 9 o’clock position to the 3 o’clock position of the 2-dimensional photon fluence rate map of the middle column of panel (C) is given at the right column.

Preprints (www.preprints.org) | NOT PEER-REVIEWED | Posted: 19 October 2018 doi:10.20944/preprints201810.0458.v1

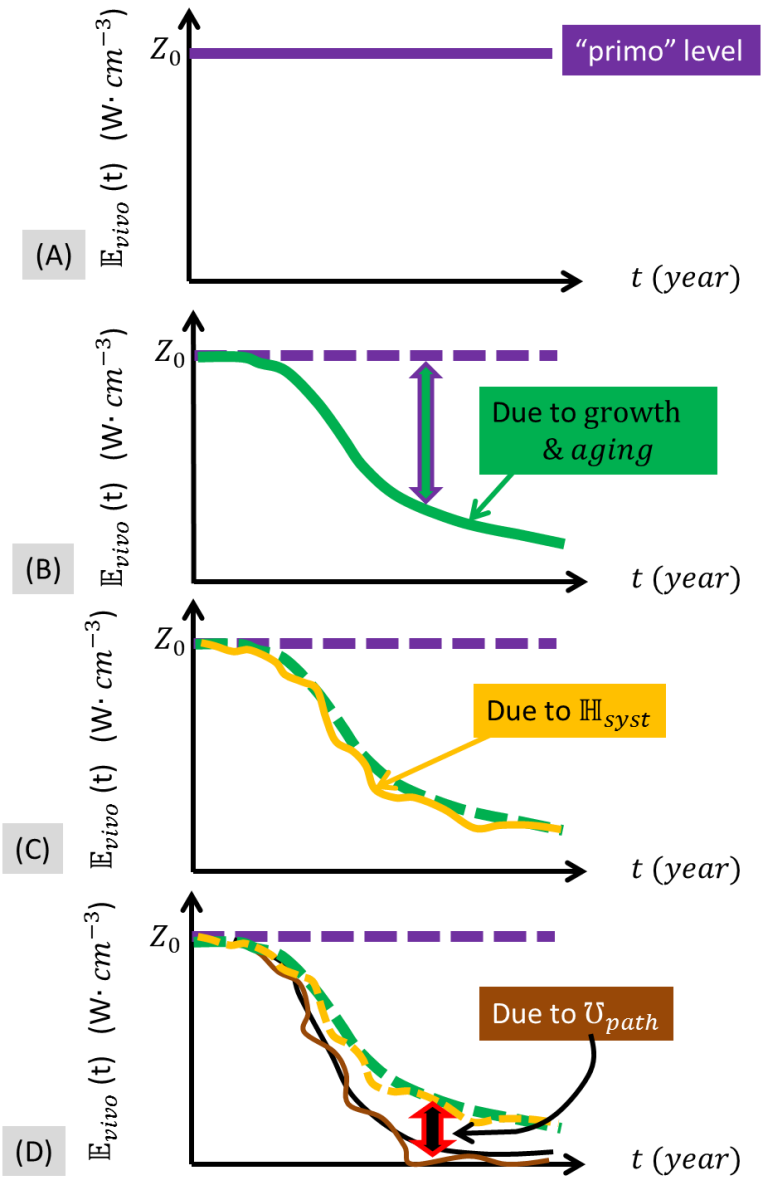

Figure 1. (A)The vivo-nergy bestowed on a person at birth. (B) The decrease of the "vivo-nergy" of a healthy person due to aging. (C) The modulation of the "vivo-nergy" of a healthy person by systematic physiology. (D) The degradation of the "vivo-nergy" of a person from the healthy level by acquired pathology.

Preprints (www.preprints.org) | NOT PEER-REVIEWED | Posted: 19 October 2018 doi:10.20944/preprints201810.0458.v1

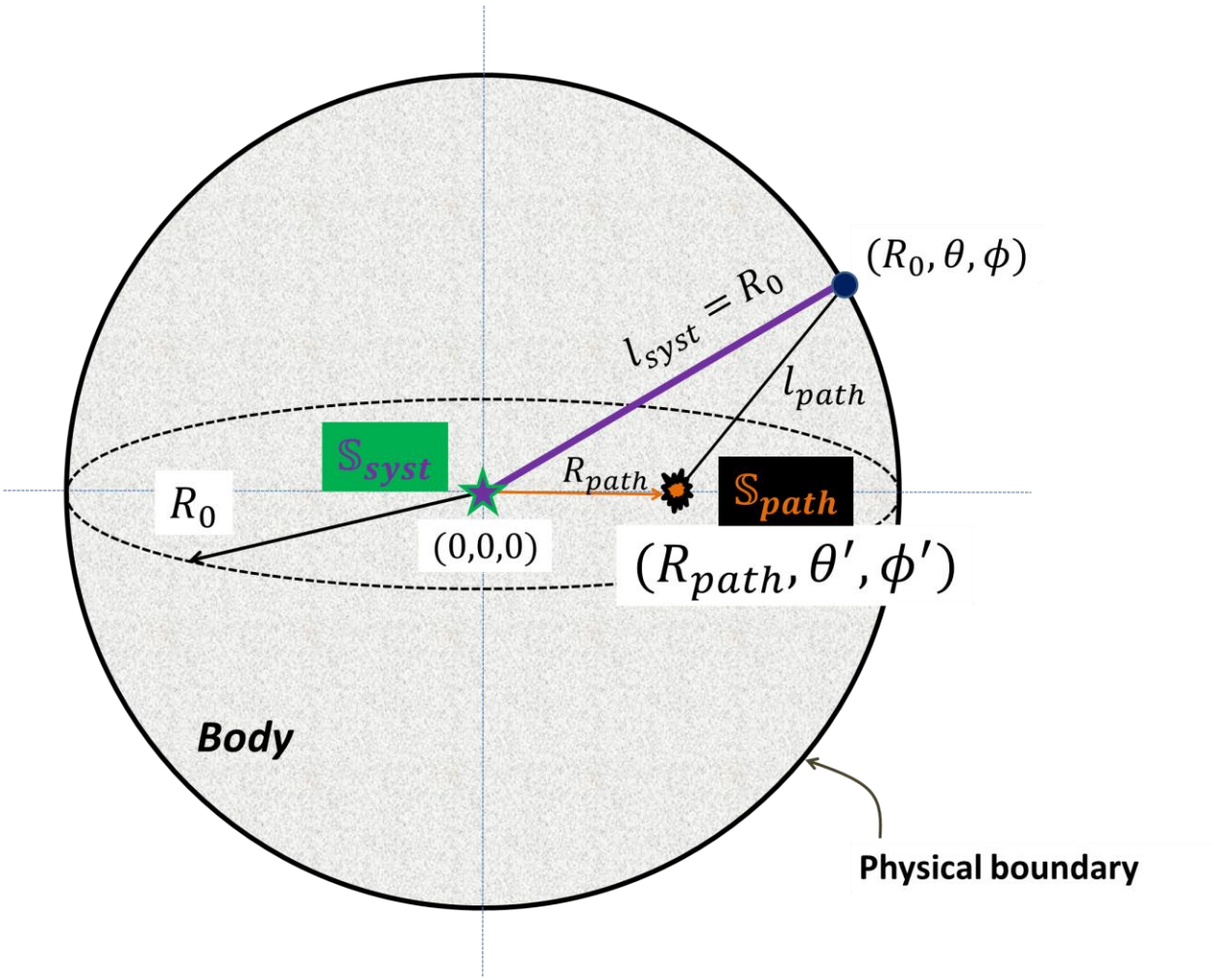

Figure 2. The human body is simplified as a spherical geometry with a radius R_0. The physiological photo-genic source $\mathbb{S}_{syst}$ is set at the center of the spherical domain, or with the spherical coordinates of (0,0,0). The pathological photo-genetic source $\mathbb{S}_{path}$ is positioned at 3 o'clock position with respect to the spherical center, at $(R_{path}, 0, 0)$. The distance of any position (R_0, θ, ϕ) on or off the spherical surface to the pathological source $\mathbb{S}_{path}$ is denoted as l_{path}.

Preprints (www.preprints.org) | NOT PEER-REVIEWED | Posted: 19 October 2018 doi:10.20944/preprints201810.0458.v1

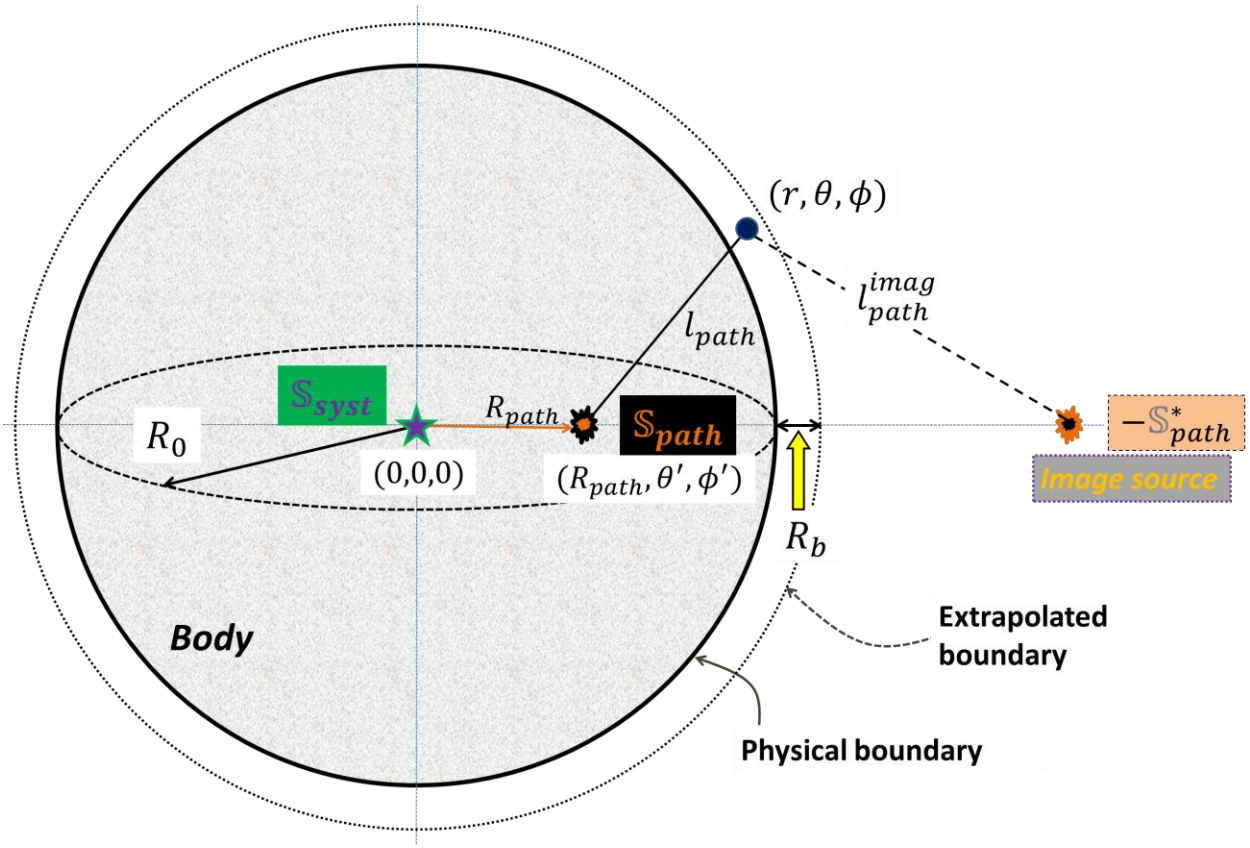

Figure 3. The human body containing a physiological photo-genic source of $\mathbb{S}_{syst}$ at the center of the spherical domain, and a single pathological photo-genetic source $\mathbb{S}_{path}$ at $(R_{path}, 0, 0)$. The photon emitted by a photo-genic source diffuses in the human body and encounters a refractive index discontinuity at the body boundary. The effect of the tissue-air boundary is accounted for by setting the photon fluence rate at an imaginary boundary extrapolated from the physical boundary at a distance of R_b. The image of the single pathological photo-genetic source $\mathbb{S}_{path}$ locates at the radial direction of $\mathbb{S}_{path}$ due to the obvious symmetry. The intensity of the image of the single pathological photo-genetic source $\mathbb{S}_{path}$ may become - $\mathbb{S}_{path}$ in the case of the tissue becoming semi-infinite domain.

Preprints (www.preprints.org) | NOT PEER-REVIEWED | Posted: 19 October 2018 doi:10.20944/preprints201810.0458.v1

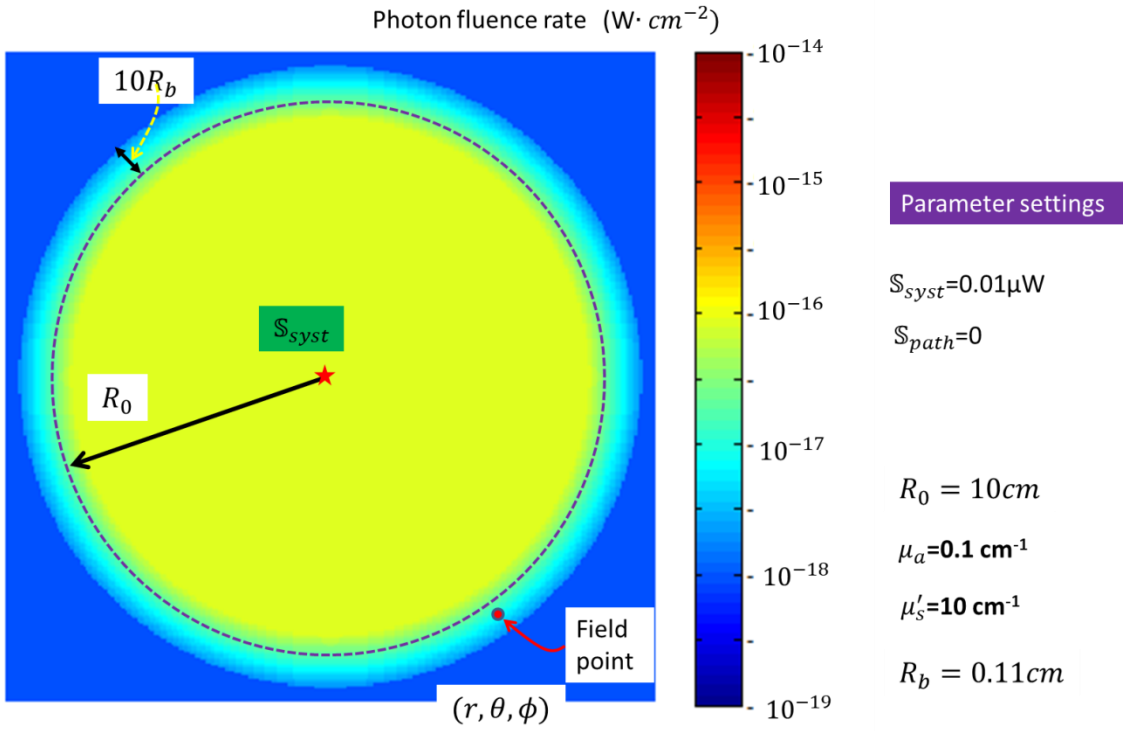

Figure 4. Example of the distribution of the photon fluence rate across the surface of the human-representing spherical domain and expanding to the extrapolated boundary. The degradation of the photon fluence rate from the tissue boundary to the extrapolated boundary over an entire azimuthal or elevational circle illustrates as a thin circular strip around the spherical tissue domain.

Preprints (www.preprints.org) | NOT PEER-REVIEWED | Posted: 19 October 2018 doi:10.20944/preprints201810.0458.v1

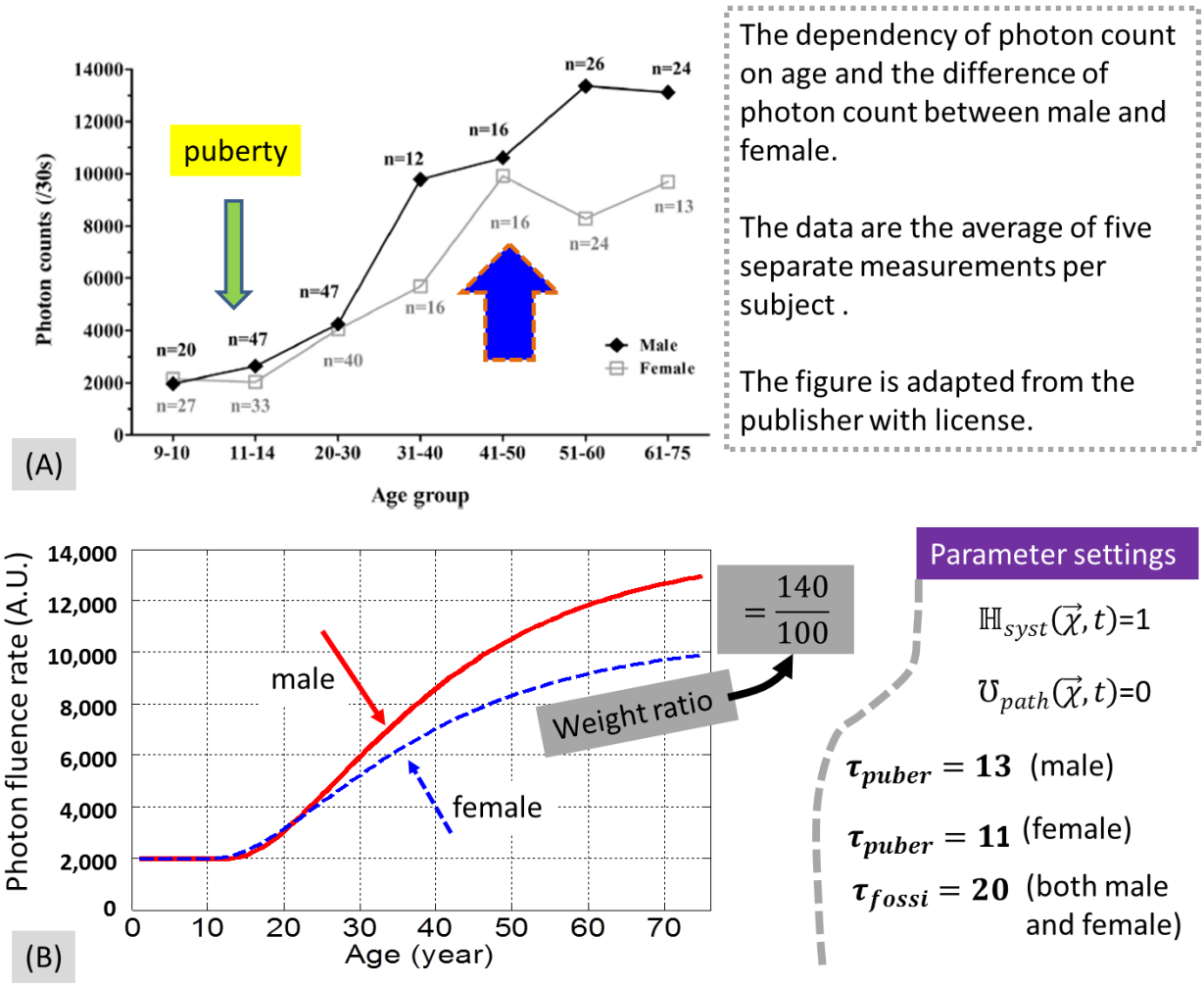

Figure 5. The age dependency and gender difference of the UPE demonstrated in a literature study [x] in (A) and the simulated photon fluence rate at the boundary of the spherical tissue domain in (B). (A) there is a smaller down-ward solid-framed arrow pointing to an age group of 11-14 of both male and female, at which the UPE photon count started to increase noticeably. That age group is projected to indicate puberty. In (A) there is a larger upward dash-framed arrow pointing to an age group of 41-50 of the female that may be interpreted as indicating menopause.

Preprints (www.preprints.org) | NOT PEER-REVIEWED | Posted: 19 October 2018 doi:10.20944/preprints201810.0458.v1

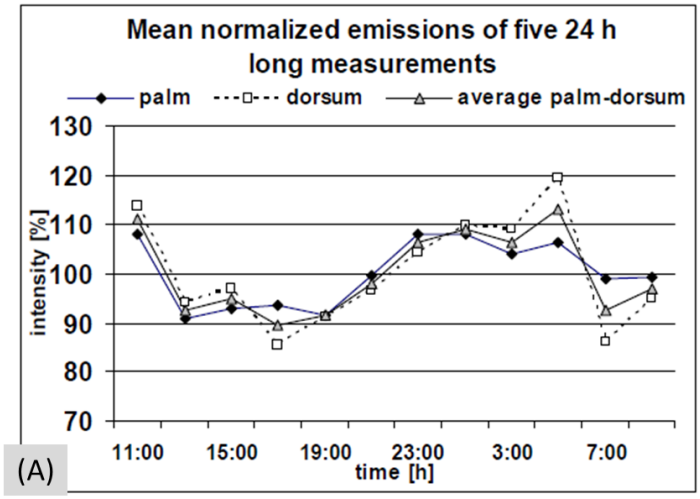

Mean normalized emissions of the five 24 h long measurements (11:00-9:00).

Every two hours left and right palm as well as dorsal sides of the left and the right hand were measured.

The data are averaged for palm and dorsal sides separately.

The figure is adopted from the open-access publication.

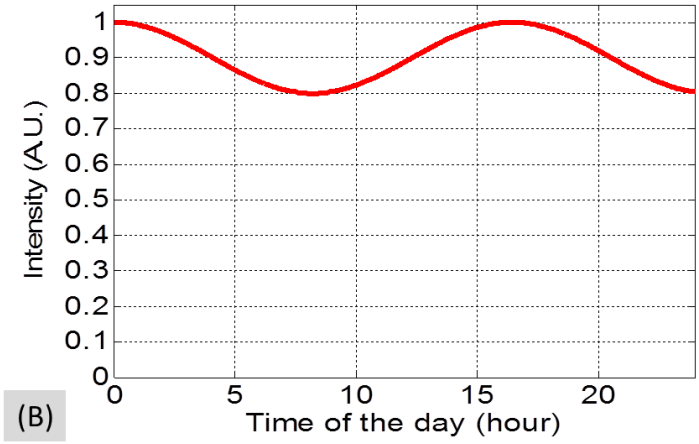

Parameter settings

$$\mathcal{V}_{path}(\vec{\chi},t)=0$$

$$\mathbb{H}_{syst}(\vec{\chi},t) = 0.9 + 0.1cos\left(\frac{\pi}{4}t - \frac{\pi}{2}\right)$$

Figure 6. A literature report showing the diurnal variation of UPE photon count is adopted from an open-access publication [41] as shown in (A). The UPE intensity revealed a trough at in later afternoon and a peak in early morning. That diurnal variation over a range of approximately 90-110% of the mid-line level can be directly associated with the circadian cycle. The variation of the photon fluence rate revealed at the boundary of the spherical tissue domain as a function of short-term homeostatic changes is simulated by removing $\mathbb{S}_{path}$ and setting the $\mathbb{H}_{syst}$ to change periodically. The circadian cycle is implemented into the intensity of physiological photo-genic source in Eq. (21) by setting $\mathbb{H}_{syst}(\vec{\chi},t) = 0.9 + 0.1cos\left(\frac{\pi}{4}t - \frac{\pi}{2}\right)$.

Preprints (www.preprints.org) | NOT PEER-REVIEWED | Posted: 19 October 2018 doi:10.20944/preprints201810.0458.v1

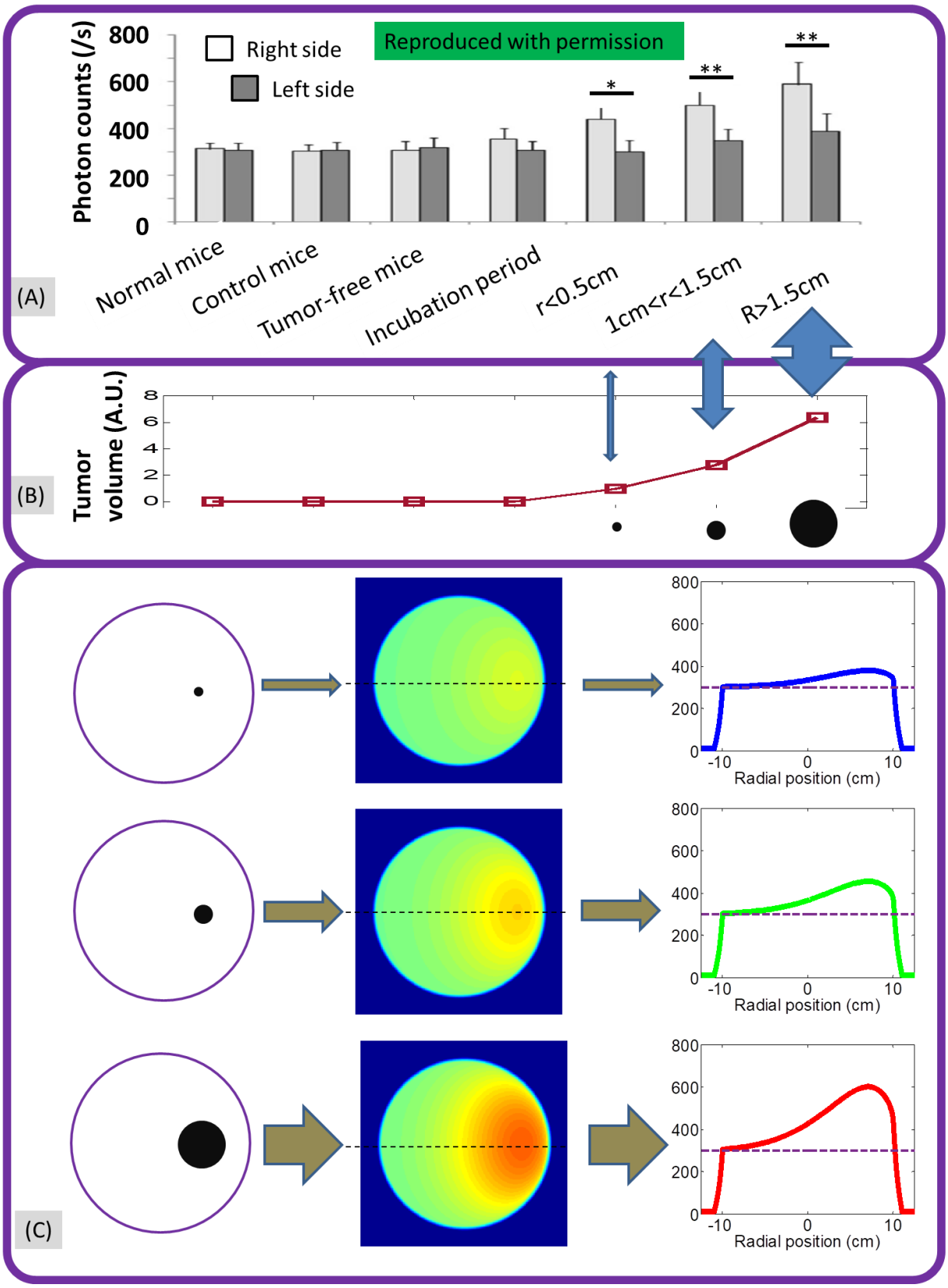

Preprints (www.preprints.org) | NOT PEER-REVIEWED | Posted: 19 October 2018 doi:10.20944/preprints201810.0458.v1

Figure 7. (A) the asymmetric UPE intensity that became aggregated as the tumor-load at the right axillary of a breast cancer mouse model increased [16]. The tumor volumes of respectively less than 0.5cm in diameter, between 1cm and 1.5cm in diameter, and greater than 1.5m in diameter as specified on panel (A) are scaled as $\exp(\frac{1}{1.5})$, $\exp(\frac{2}{1.5})$, and $\exp(\frac{3}{1.5})$ as plotted on the panel (B). The resulted numerical value of the tumor size is scaled to 1% and used as the intensity of the pathological photo-genic source $\mathbb{S}_{path}$ that is placed at 1cm off the center at the right-lateral aspect and 1cm off center at the right anterior aspect, as illustrated in the left column of panel (C). The resulted photon fluence rate over the surface of the spherical tissue domain that is projected to the middle cross-section and surrounded by a thin strip of the space beyond the tissue boundary is presented in the middle column of panel (C). The 1-dimentional profile along the diameter crossing the 9 o'clock position to the 3 o'clock position of the 2-dimensional photon fluence rate map of the middle column of panel (C) is given at the right column.

References

1. Cifra, M. and P. Pospisil, *Ultra-weak photon emission from biological samples: definition, mechanisms, properties, detection and applications.* J Photochem Photobiol B, 2014. **139**: p. 2-10.
2. Quickenden, T.I. and S.S. Que Hee, *Weak luminescence from the yeast Saccharomyces cerevisiae and the existence of mitogenetic radiation.* Biochem Biophys Res Commun, 1974. **60**(2): p. 764-70.
3. Cadenas, E., A. Boveris, and B. Chance, *Low-level chemiluminescence of bovine heart submitochondrial particles.* Biochem J, 1980. **186**(3): p. 659-67.
4. Boveris, A., et al., *Spontaneous Chemiluminescence of Soybean Embryonic Axes during Imbibition.* Plant Physiol, 1984. **76**(2): p. 447-51.
5. Devaraj, B., M. Usa, and H. Inaba, *Biophotons: Ultraweak light emission from living systems.* Current Opinion in Solid State & Materials Science, 1997. **2**(2): p. 188-193.
6. Cohen, S. and F.A. Popp, *Biophoton emission of the human body.* J Photochem Photobiol B, 1997. **40**(2): p. 187-9.
7. Wang, J. and Y. Yu, *Relationship between ultra-weak bioluminescence and vigour or irradiation dose of irradiated wheat.* Luminescence, 2009. **24**(4): p. 209-12.
8. Havaux, M., C. Triantaphylides, and B. Genty, *Autoluminescence imaging: a non-invasive tool for mapping oxidative stress.* Trends Plant Sci, 2006. **11**(10): p. 480-4.
9. Moraes, T.A., et al., *Spontaneous ultra-weak light emissions from wheat seedlings are rhythmic and synchronized with the time profile of the local gravimetric tide.* Naturwissenschaften, 2012. **99**(6): p. 465-72.
10. Boveris, A., et al., *Organ chemiluminescence: noninvasive assay for oxidative radical reactions.* Proc Natl Acad Sci U S A, 1980. **77**(1): p. 347-51.
11. Cadenas, E., *Biological chemiluminescence.* Photochem Photobiol, 1984. **40**(6): p. 823-30.
12. Gallas, J.M. and M. Eisner, *Fluorescence of Melanin Dependence Upon Excitation Wavelength and Concentration.* Photochemistry and Photobiology, 1987. **45**(5): p. 595-600.
13. Kayatz, P., et al., *Oxidation causes melanin fluorescence.* Invest Ophthalmol Vis Sci, 2001. **42**(1): p. 241-6.
14. Kalaji, H.M., et al., *Experimental in vivo measurements of light emission in plants: a perspective dedicated to David Walker.* Photosynthesis Research, 2012. **114**(2): p. 69-96.
15. Fedorova, G.F., et al., *Peroxy-radical-mediated chemiluminescence: mechanistic diversity and fundamentals for antioxidant assay.* Arkivoc, 2007: p. 163-215.
16. Zhao, X., et al., *Spontaneous photon emission: A promising non-invasive diagnostic tool for breast cancer.* J Photochem Photobiol B, 2017. **166**: p. 232-238.
17. Kobayashi, M., T. Iwasa, and M. Tada, *Polychromatic spectral pattern analysis of ultra-weak photon emissions from a human body.* J Photochem Photobiol B, 2016. **159**: p. 186-90.
18. Wang, Z., et al., *Human high intelligence is involved in spectral redshift of biophotonic activities in the brain.* Proc Natl Acad Sci U S A, 2016. **113**(31): p. 8753-8.
19. Nakamura, K. and M. Hiramatsu, *Ultra-weak photon emission from human hand: influence of temperature and oxygen concentration on emission.* J Photochem Photobiol B, 2005. **80**(2): p. 156-60.

20. Jung, H.H., et al., *Year-long biophoton measurements: normalized frequency count analysis and seasonal dependency.* J Photochem Photobiol B, 2005. **78**(2): p. 149-54.
21. Ou-Yang, H., *The application of ultra-weak photon emission in dermatology.* J Photochem Photobiol B, 2014. **139**: p. 63-70.
22. Zhao, X., et al., *Ultra-weak photon emission of hands in aging prediction.* J Photochem Photobiol B, 2016. **162**: p. 529-534.
23. Cadenas, E., et al., *Partial spectral analysis of the hydroperoxide-induced chemiluminescence of the perfused lung.* FEBS Lett, 1980. **111**(2): p. 413-8.
24. Kobayashi, M., D. Kikuchi, and H. Okamura, *Imaging of ultraweak spontaneous photon emission from human body displaying diurnal rhythm.* PLoS One, 2009. **4**(7): p. e6256.
25. Cohen, S. and F.A. Popp, *Biophoton emission of human body.* Indian J Exp Biol, 2003. **41**(5): p. 440-5.
26. Zheng R, L.J., Lin Y et al. , *The studies of the relationship between human body surface ultraweak luminescence and certain physiological state.* Shanghai Zhongyiyao Zazhi, 1983. **1**(1): p. 44-47.
27. He, M., et al., *A Chinese literature overview on ultra-weak photon emission as promising technology for studying system-based diagnostics.* Complement Ther Med, 2016. **25**: p. 20-6.
28. Sauermann, G., et al., *Ultraweak photon emission of human skin in vivo: influence of topically applied antioxidants on human skin.* Methods Enzymol, 1999. **300**: p. 419-28.
29. Yang W, Z.W., Song W, et al., *Ultraweak photon emission experimentalstudy on the four limbs meridian of 130 healthy people.* Shanghai ZhenjiuZazhi., 1996. **15**(1): p. 34-35.
30. Yang W, Z.W., Lv Y, et al., *Ultraweak photon emission experimental study on the torso meridian of 80 healthy people.* Shenzhen Zhongxiyi Jiehe Zazhi, 1995. **5**(3): p. 1-3.
31. Sun, M., et al., *Measuring ultra-weak photon emission as a non-invasive diagnostic tool for detecting early-stage type 2 diabetes: A step toward personalized medicine.* J Photochem Photobiol B, 2017. **166**: p. 86-93.
32. Jung, H.H., et al., *Left-right asymmetry of biophoton emission from hemiparesis patients.* Indian J Exp Biol, 2003. **41**(5): p. 452-6.
33. Ives, J.A., et al., *Ultraweak photon emission as a non-invasive health assessment: a systematic review.* PLoS One, 2014. **9**(2): p. e87401.
34. Slawinski, J., et al., *Stress-induced photon emission from perturbed organisms.* Experientia, 1992. **48**(11-12): p. 1041-58.
35. Burgos, R.C., et al., *Tracking biochemical changes correlated with ultra-weak photon emission using metabolomics.* J Photochem Photobiol B, 2016. **163**: p. 237-45.
36. Ishimaru, A., *Diffusion of light in turbid material.* Appl Opt, 1989. **28**(12): p. 2210-5.
37. Contini, D., F. Martelli, and G. Zaccanti, *Photon migration through a turbid slab described by a model based on diffusion approximation. I. Theory.* Appl Opt, 1997. **36**(19): p. 4587-99.
38. Zhang, A., et al., *Photon diffusion in a homogeneous medium bounded externally or internally by an infinitely long circular cylindrical applicator. I. Steady-state theory.* J Opt Soc Am A Opt Image Sci Vis, 2010. **27**(3): p. 648-62.
39. Piao, D., et al., *On the geometry dependence of differential pathlength factor for near-infrared spectroscopy. I. Steady-state with homogeneous medium.* J Biomed Opt, 2015. **20**(10): p. 105005.

40. Haskell, R.C., et al., *Boundary conditions for the diffusion equation in radiative transfer.* J Opt Soc Am A Opt Image Sci Vis, 1994. **11**(10): p. 2727-41.
41. CIFRA M, V.W.E., KOCH H, BOSMAN s, VAN WIJK R., *Spontaneous Ultra-Weak Photon Emission from Human Hands Is Time Dependent.* RADIOENGINEERING, 2007. **16**(2): p. 15-19.
42. Jiang, Z., et al., *Transrectal ultrasound-integrated spectral optical tomography of hypoxic progression of a regressing tumor in a canine prostate.* Technol Cancer Res Treat, 2011. **10**(6): p. 519-31.
43. Van Wijk, R., et al., *Towards whole-body ultra-weak photon counting and imaging with a focus on human beings: a review.* J Photochem Photobiol B, 2014. **139**: p. 39-46.
44. Arridge, S.R., et al., *The finite element model for the propagation of light in scattering media: a direct method for domains with nonscattering regions.* Med Phys, 2000. **27**(1): p. 252-64.